Supplementary Figures

The citrate transporters SLC13A5 and SLC25A1 elicit different metabolic responses and phenotypes in the mouse

Gonzalo Fernandez-Fuente[1,2], Katherine A. Overmyer[3,4], Alexis J. Lawton[3,5], Ildiko Kasza[6], Samantha L. Shapiro[1,2], Patricia Gallego-Muñoz[7], Joshua J. Coon[3,4,8], John M. Denu[3,5], Caroline M. Alexander[6], Luigi Puglielli[1,2,9,10,*]

[1]Department of Medicine, University of Wisconsin-Madison, Madison, WI, USA
[2]Waisman Center, University of Wisconsin-Madison, Madison, WI, USA
[3]Department of Biomolecular Chemistry, University of Wisconsin-Madison, Madison, WI, USA
[4]Morgridge Institute for Research, Madison, WI, USA
[5]Wisconsin Institute for Discovery, University of Wisconsin-Madison, Madison, WI, USA
[6]McArdle Laboratory for Cancer Research, University of Wisconsin-Madison, Madison, WI, USA
[7]Department of Cell Biology, Genetics, Histology and Pharmacology, Faculty of Medicine, University of Valladolid, Valladolid, Spain
[8]Department of Chemistry, University of Wisconsin-Madison, Madison, WI, USA
[9]Geriatric Research Education Clinical Center, Veterans Affairs Medical Center, Madison, WI, USA
[10]Department of Neuroscience, University of Wisconsin-Madison, Madison, WI, USA

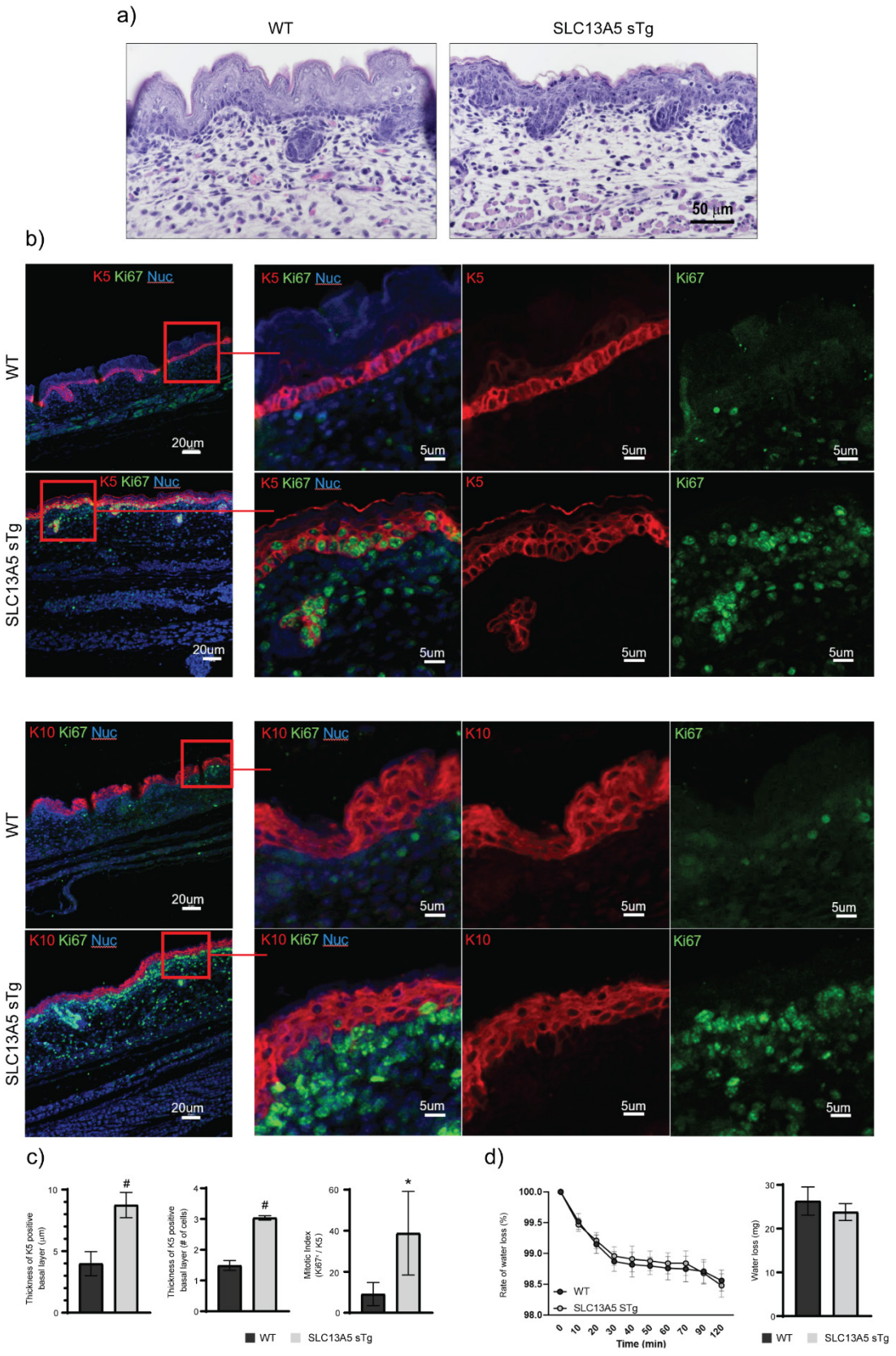
a)
WT
SLC13A5 sTg
50 μm
b)
WT
SLC13A5 sTg
K5 Ki67 Nuc
K5
Ki67
K10 Ki67 Nuc
K10
20um
5um
c)
Thickness of K5 positive basal layer (μm)
Thickness of K5 positive basal layer (# of cells)
Mitotic Index (Ki67+ / K5)
#
*
WT
SLC13A5 sTg
d)
Rate of water loss (%)
Time (min)
Water loss (mg)
WT
SLC13A5 STg

Supplementary Figure 1. SLC13A5 sTg^{OC} mice display skin defects before birth (E18).

(a) Representative H&E staining of skin sections from WT and SLC13A5 sTg^{OC} embryos.

(b) Immunostaining of 5µm paraffin-embedded skin slices from WT and SLC13A5 sTg^{OC} embryos. Keratin 5 (upper panel) and Keratin 10 (lower panel) combined with proliferation marker Ki67 and nuclear staining.

(c) Keratin 5 basal layer thickness (µm and number of cells) and Mitotic index (n=3/group). *P<0.05, $^{\#}P$<0.0005 via mean comparison using Student's t-test.

(d) Water loss expressed as percentage rate over time and total milligrams (n=8 WT; n=5 SLC13A5 sTg mice).

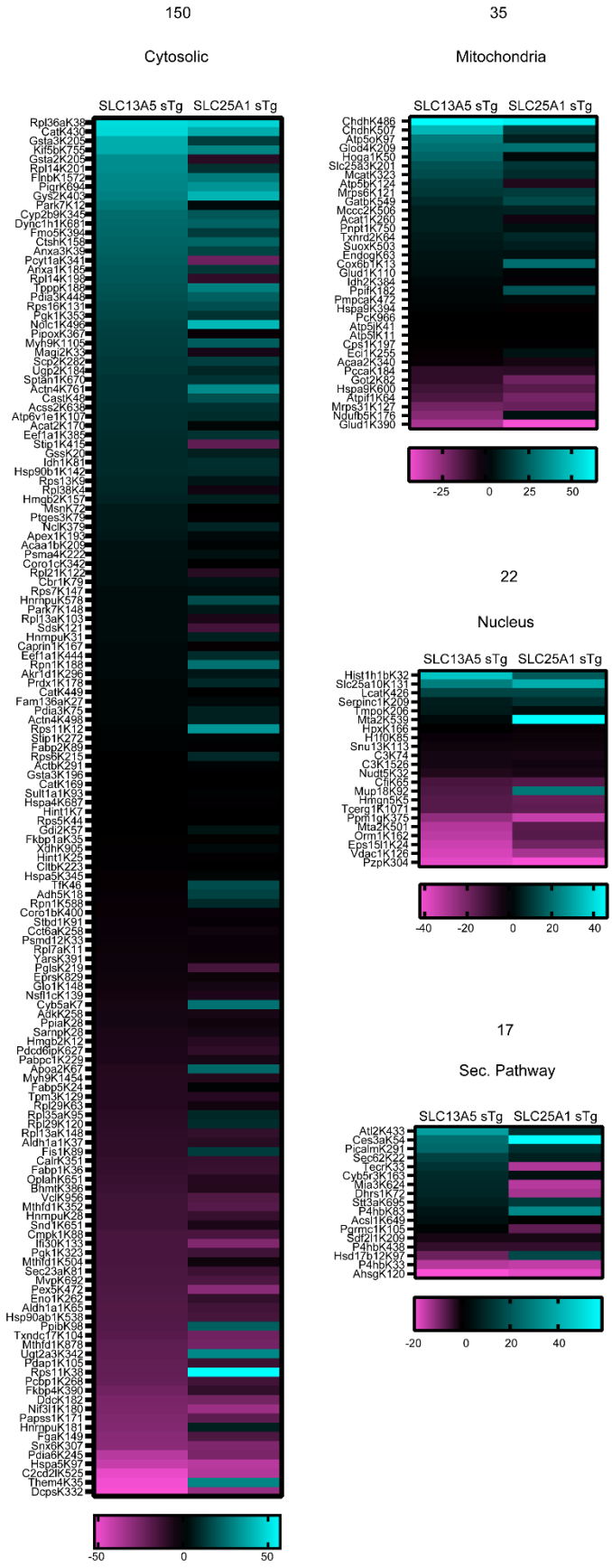
150
Cytosolic
SLC13A5 sTg
SLC25A1 sTg
-50
0
50
35
Mitochondria
SLC13A5 sTg
SLC25A1 sTg
-25
0
25
50
22
Nucleus
SLC13A5 sTg
SLC25A1 sTg
-40
-20
0
20
40
17
Sec. Pathway
SLC13A5 sTg
SLC25A1 sTg
-20
0
20
40

Supplementary Figure 2. Heat-maps showing the profile of the 224 overlapping acetylation sites among the cytosolic, mitochondria, nucleus, and secretory pathway fractions found in both SLC13A5 sTg and SLC25A1 sTg mice, as compared to WT littermates. Mice were 2 month-old when analyzed.

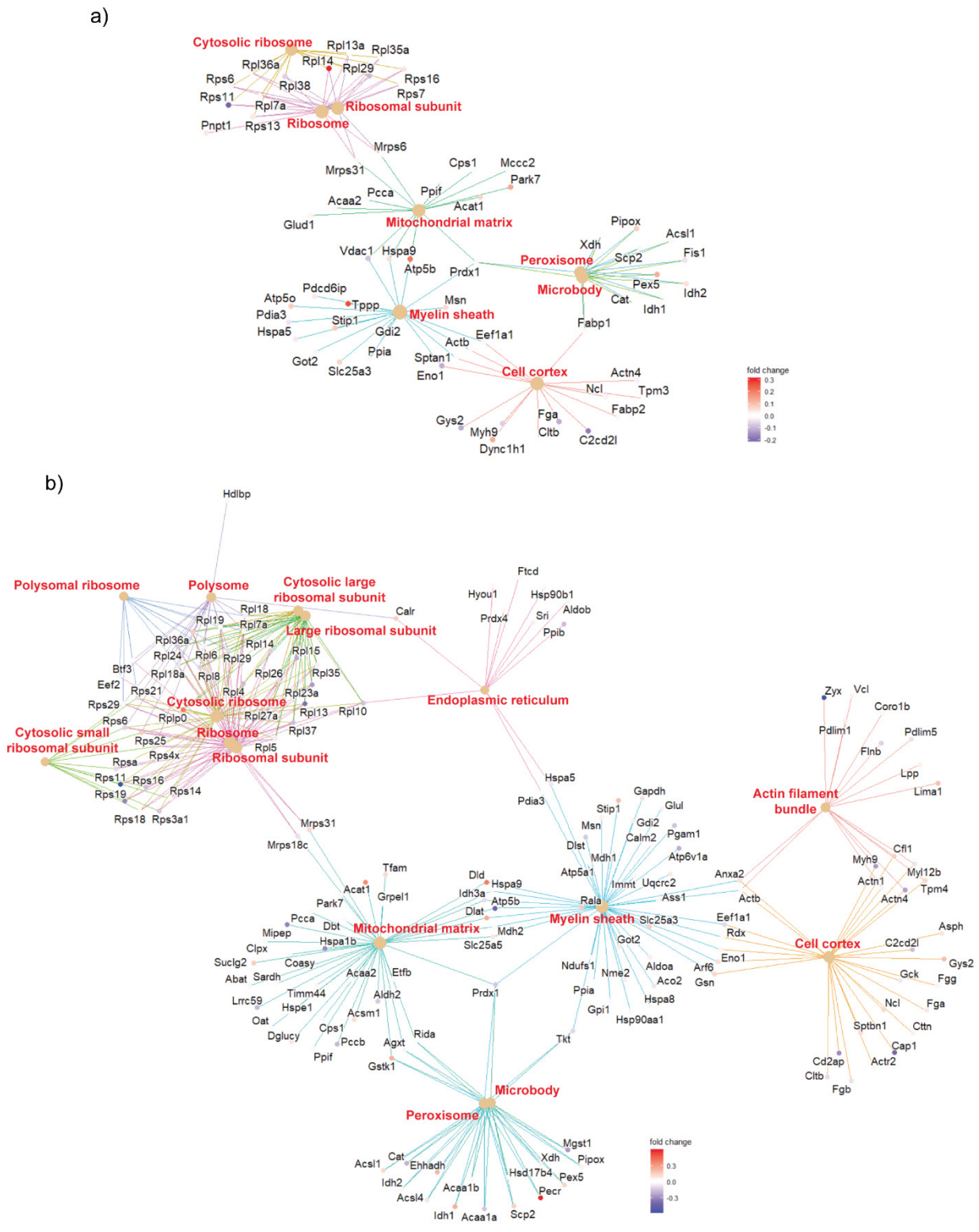
a)
Cytosolic ribosome
Rpl13a
Rpl35a
Rpl36a
Rpl14
Rpl29
Rps6
Rpl38
Rps16
Rps11
Rps7
Rpl7a
Ribosomal subunit
Pnpt1
Rps13
Ribosome
Mrps6
Mrps31
Cps1
Mccc2
Park7
Acaa2
Pcca
Ppif
Acat1
Glud1
Mitochondrial matrix
Pipox
Acsl1
Xdh
Fis1
Vdac1
Hspa9
Scp2
Peroxisome
Atp5b
Prdx1
Pex5
Idh2
Microbody
Cat
Idh1
Pdcd6ip
Atp5o
Tppp
Msn
Pdia3
Stip1
Myelin sheath
Fabp1
Hspa5
Gdi2
Eef1a1
Actb
Ppia
Got2
Sptan1
Slc25a3
Eno1
Cell cortex
Actn4
Ncl
Tpm3
Fabp2
Gys2
Fga
Myh9
Cltb
C2cd2l
Dync1h1
fold change
0.3
0.2
0.1
0.0
-0.1
-0.2
b)
Hdlbp
Polysomal ribosome
Polysome
Cytosolic large ribosomal subunit
Rpl18
Rpl19
Rpl7a
Calr
Large ribosomal subunit
Rpl36a
Rpl14
Rpl15
Rpl24
Rpl6
Rpl29
Btf3
Rpl18a
Rpl8
Rpl26
Rpl35
Eef2
Rps21
Rpl4
Rpl23a
Rps29
Cytosolic ribosome
Rpl27a
Rpl13
Rpl10
Rps6
Rplp0
Cytosolic small ribosomal subunit
Ribosome
Rpl37
Rps25
Rpl5
Rps4x
Ribosomal subunit
Rpsa
Rps11
Rps16
Rps19
Rps14
Rps18
Rps3a1
Ftcd
Hyou1
Hsp90b1
Prdx4
Sri
Aldob
Ppib
Endoplasmic reticulum
Mrps31
Mrps18c
Tfam
Acat1
Grpel1
Park7
Pcca
Mipep
Dbt
Mitochondrial matrix
Hspa1b
Clpx
Suclg2
Coasy
Abat
Sardh
Acaa2
Etfb
Lrrc59
Timm44
Aldh2
Hspe1
Oat
Acsm1
Cps1
Dglucy
Pccb
Agxt
Rida
Ppif
Gstk1
Hspa5
Pdia3
Gapdh
Stip1
Glul
Msn
Gdi2
Pgam1
Calm2
Dlst
Mdh1
Atp6v1a
Atp5a1
Dld
Hspa9
Idh3a
Atp5b
Dlat
Mdh2
Slc25a5
Immt
Uqcrc2
Rala
Ass1
Myelin sheath
Slc25a3
Got2
Ndufs1
Nme2
Aldoa
Aco2
Ppia
Hspa8
Gpi1
Hsp90aa1
Prdx1
Tkt
Microbody
Peroxisome
Mgst1
Xdh
Pipox
Acsl1
Cat
Ehhadh
Hsd17b4
Pex5
Idh2
Acsl4
Acaa1b
Pecr
Idh1
Acaa1a
Scp2
Anxa2
Actb
Eef1a1
Rdx
Eno1
Arf6
Gsn
Actin filament bundle
Zyx
Vcl
Coro1b
Pdlim1
Pdlim5
Flnb
Lpp
Lima1
Cfl1
Myh9
Myl12b
Actn1
Tpm4
Actn4
Cell cortex
Asph
C2cd2l
Gys2
Gck
Fgg
Ncl
Fga
Sptbn1
Cttn
Cap1
Cd2ap
Actr2
Cltb
Fgb
fold change
0.3
0.0
-0.3

Supplementary Figure 3. STRING analysis of unique changes in stoichiometry of lysine acetylation.

(a) Gene-network plot of proteins (total of 193) harboring the acetylation sites that were significantly changed from WT and shared by SLC13A5 and SLC25A1 sTg mice. Plot constructed via an overrepresentation analysis using the GO cellular component function database. The color of each dot indicates the fold change in the stoichiometry of lysine acetylation. The top 8 categories sorted by enrichment score are shown with a filtered FDR score of 0.05.

(b) Gene-network plot of proteins (total of 500) harboring the acetylation sites that were significantly changed in SLC13A5 mice, as compared to SLC25A1 sTg mice. Plot constructed via an overrepresentation analysis using the GO cellular component function database. The color of each dot indicates the fold change in the stoichiometry of lysine acetylation. The top 15 categories sorted by enrichment score are shown with a filtered FDR score of 0.05.

Mice were 2 month-old when analyzed.

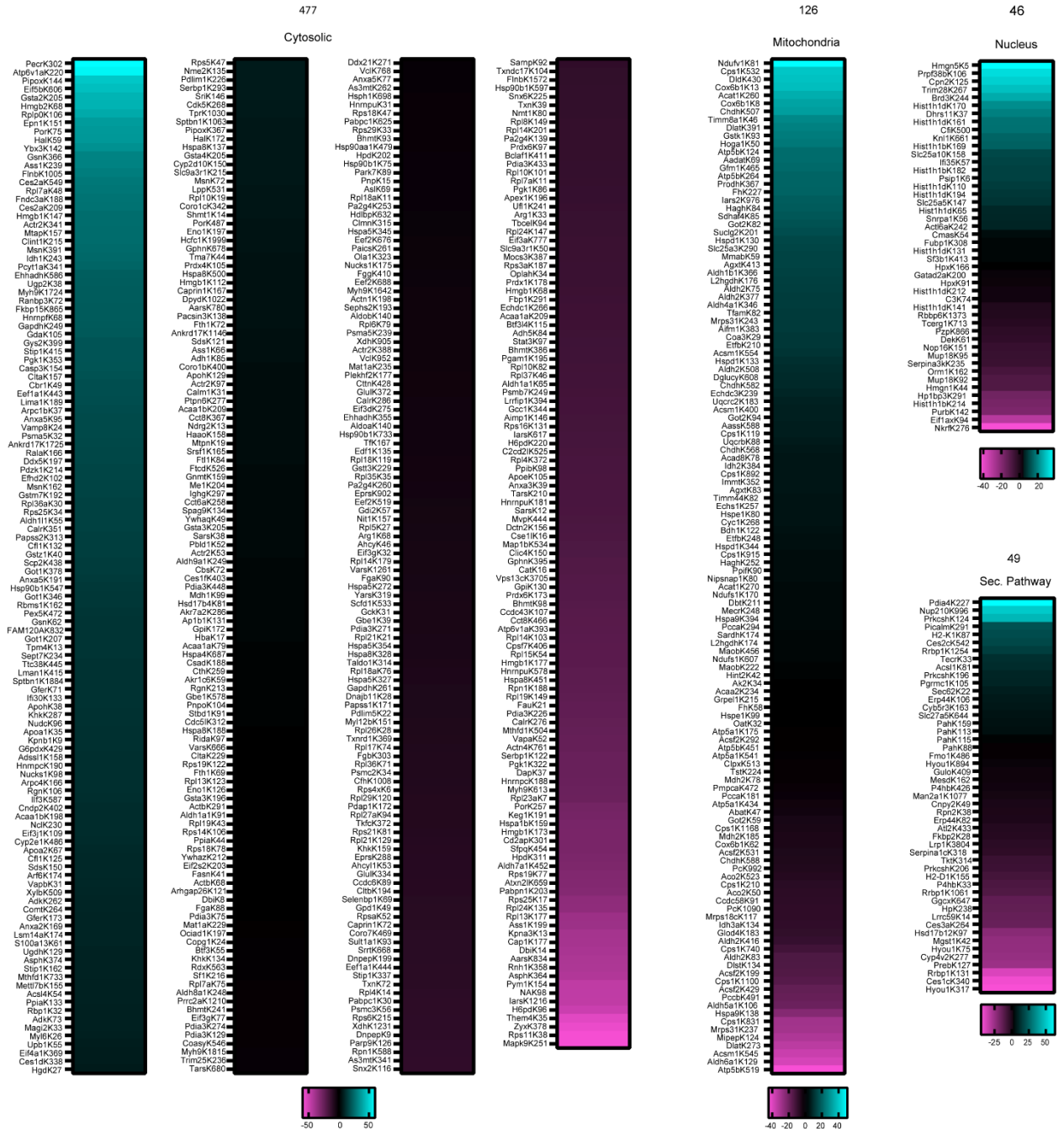
477
Cytosolic
126
Mitochondria
46
Nucleus
49
Sec. Pathway

Supplementary Figure 4. Heat-maps showing the profile of the 698 acetylation sites among the cytosolic, mitochondria, nucleus, and secretory pathway fractions found in SLC13A5 sTg mice, as compared to SLC25A1 sTg mice. Mice were 2 month-old when analyzed.

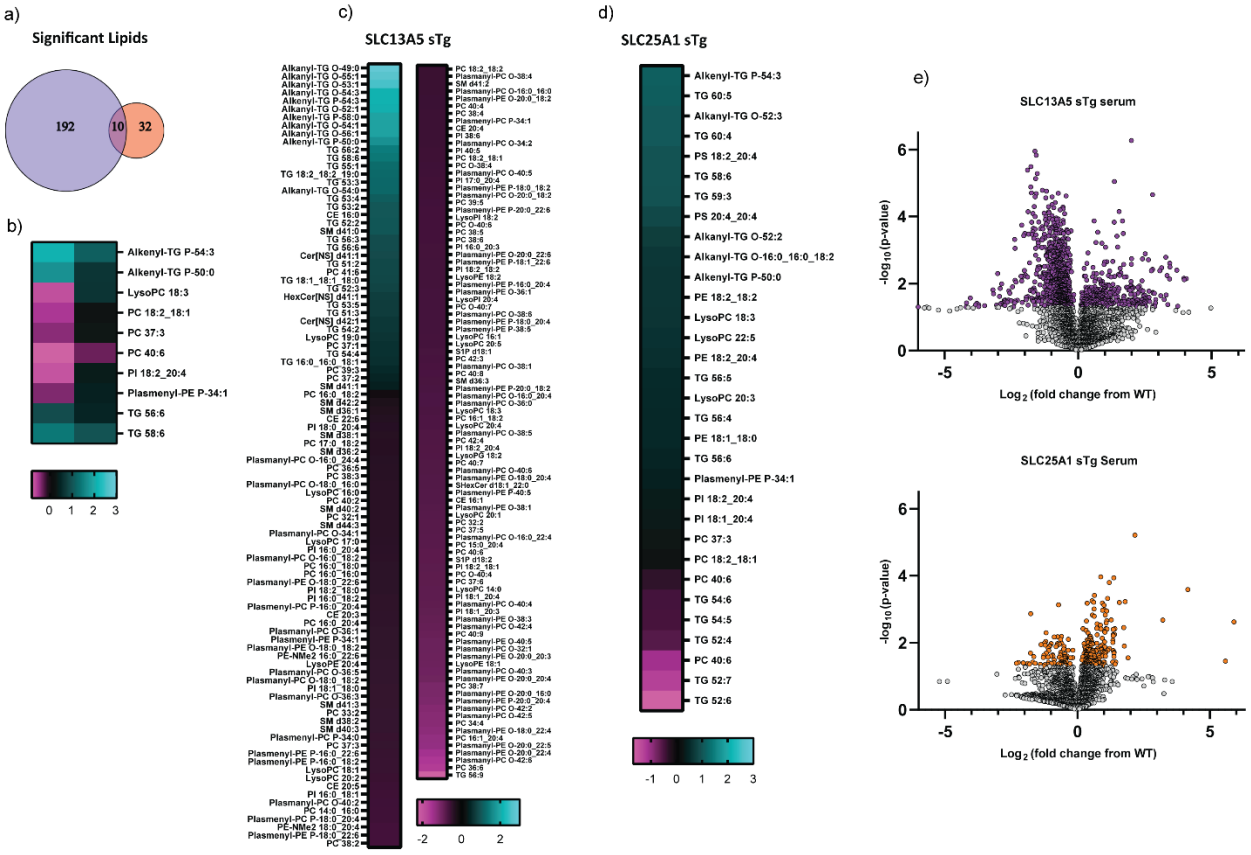
a)
Significant Lipids
192
10
32
b)
Alkenyl-TG P-54:3
Alkenyl-TG P-50:0
LysoPC 18:3
PC 18:2_18:1
PC 37:3
PC 40:6
PI 18:2_20:4
Plasmenyl-PE P-34:1
TG 56:6
TG 58:6
0 1 2 3
c)
SLC13A5 sTg
-2 0 2
d)
SLC25A1 sTg
-1 0 1 2 3
e)
SLC13A5 sTg serum
-log10 (p-value)
Log2 (fold change from WT)
SLC25A1 sTg Serum
-log10 (p-value)
Log2 (fold change from WT)

Supplementary Figure 5. SLC13A5 sTg and SLC25A1 sTg mice display different lipid adaptation in the serum.

(a) Venn diagram showing overlap between SLC13A5 sTg (purple) and SLC25A1 sTg (orange) mice across statistically significant lipids (n=5 male mice per group).

(b) Heat-map showing the expression profile of dysregulated lipids (total of 10) found in SLC13A5 sTg and SLC25A1 sTg mice, as compared to WT littermates.

(c) Heat-map showing the expression profile of dysregulated lipids (total of 192) found in SLC13A5 sTg mice, as compared to WT littermates.

(d) Heat-map showing the expression profile of dysregulated lipids (total of 32) found in SLC25A1 sTg mice, as compared to WT littermates.

(e) Volcano plots displaying all quantified lipids in SLC13A5 sTg and SLC25A1 sTg blood serum, as compared to age-matched WT littermates. Statistically significant species are highlighted in purple (for SLC13A5 sTg) and orange (for SLC25A1 sTg). $P<0.05$ via Fisher's method with all other species in grey.

Mice were 2 month-old when analyzed.

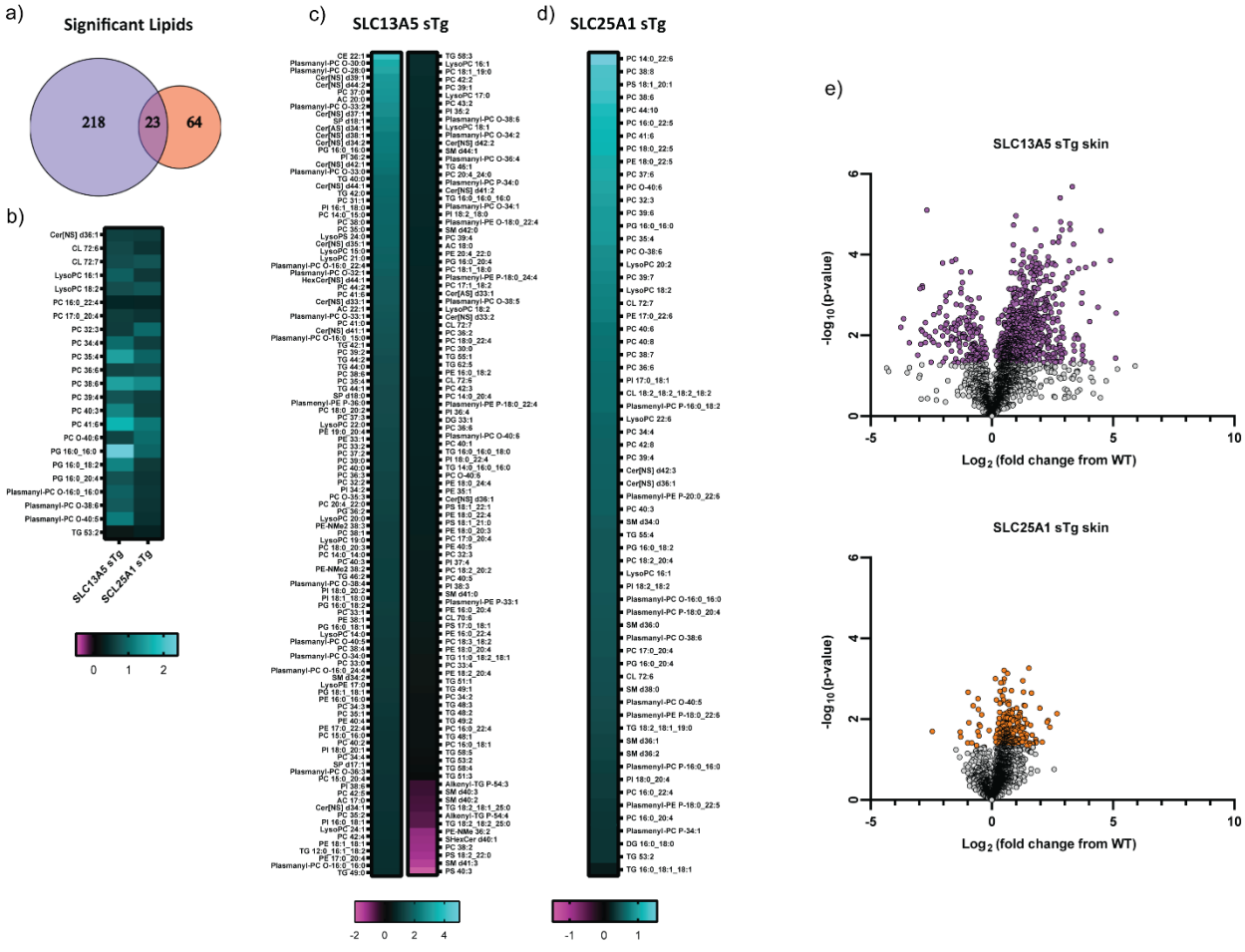
a)
Significant Lipids
218
23
64
b)
SLC13A5 sTg
SCL25A1 sTg
0
1
2
c)
SLC13A5 sTg
-2
0
2
4
d)
SLC25A1 sTg
-1
0
1
e)
SLC13A5 sTg skin
-log10 (p-value)
Log2 (fold change from WT)
SLC25A1 sTg skin
-log10 (p-value)
Log2 (fold change from WT)

Supplementary Figure 6. SLC13A5 sTg and SLC25A1 sTg mice display different lipid adaptation in the skin.

(a) Venn diagram showing overlap between SLC13A5 sTg (purple) and SLC25A1 sTg (orange) mice across statistically significant lipids (n=5 male mice per group).

(b) Heat-map showing the expression profile of dysregulated lipids (total of 23) found in SLC13A5 sTg and SLC25A1 sTg mice, as compared to WT littermates.

(c) Heat-map showing the expression profile of dysregulated lipids (total of 218) found in SLC13A5 sTg mice, as compared to WT littermates.

(d) Heat-map showing the expression profile of dysregulated lipids (total of 64) found in SLC25A1 sTg mice, as compared to WT littermates.

(e) Volcano plots displaying all quantified lipids in SLC13A5 sTg and SLC25A1 sTg skin tissue, as compared to age-matched WT littermates. Statistically significant species are highlighted in purple (for SLC13A5 sTg) and orange (for SLC25A1 sTg). $P<0.05$ via Fisher's method with all other species in grey.

Mice were 2 month-old when analyzed.

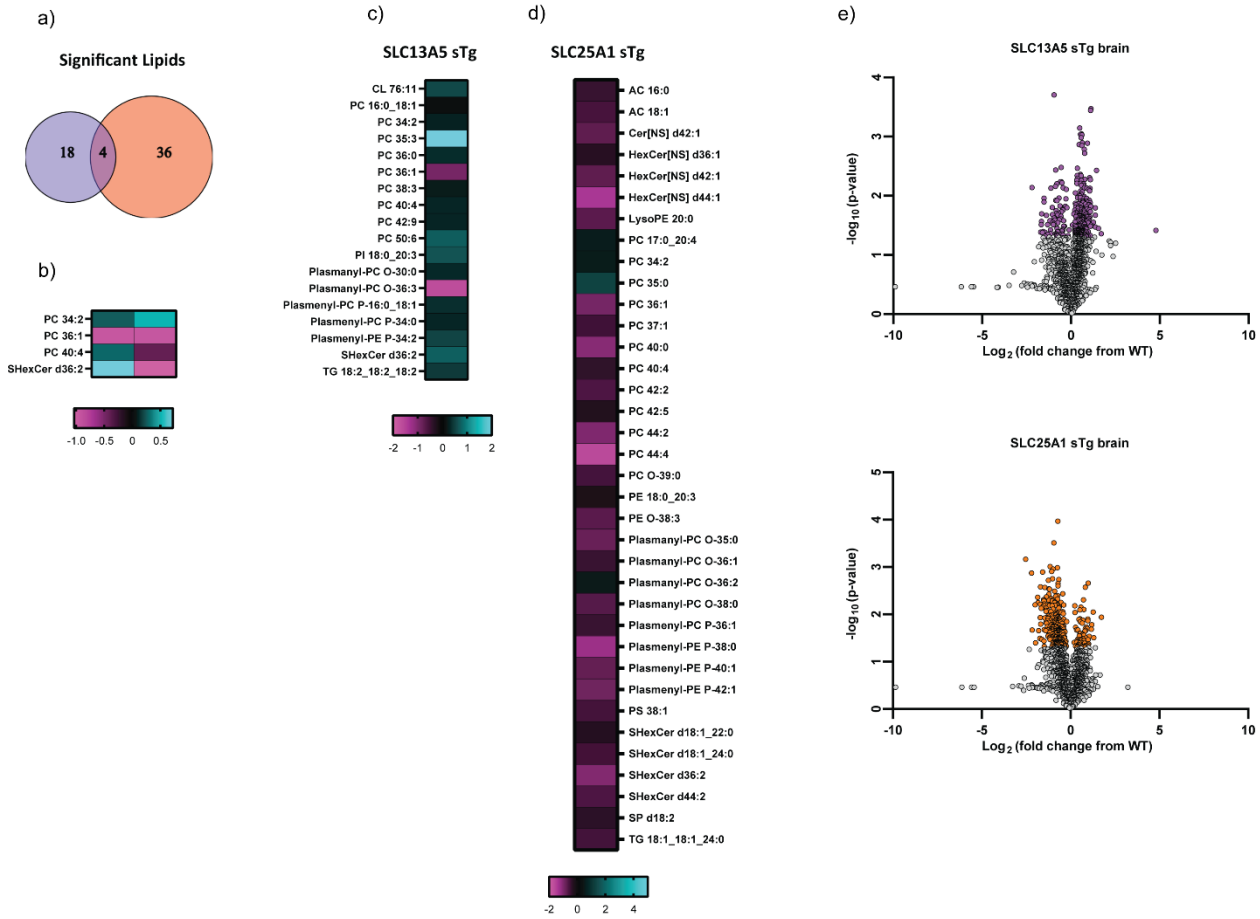
a)
Significant Lipids
18
4
36
b)
PC 34:2
PC 36:1
PC 40:4
SHexCer d36:2
-1.0 -0.5 0 0.5
c)
SLC13A5 sTg
CL 76:11
PC 16:0_18:1
PC 34:2
PC 35:3
PC 36:0
PC 36:1
PC 38:3
PC 40:4
PC 42:9
PC 50:6
PI 18:0_20:3
Plasmanyl-PC O-30:0
Plasmanyl-PC O-36:3
Plasmenyl-PC P-16:0_18:1
Plasmenyl-PC P-34:0
Plasmenyl-PE P-34:2
SHexCer d36:2
TG 18:2_18:2_18:2
-2 -1 0 1 2
d)
SLC25A1 sTg
AC 16:0
AC 18:1
Cer[NS] d42:1
HexCer[NS] d36:1
HexCer[NS] d42:1
HexCer[NS] d44:1
LysoPE 20:0
PC 17:0_20:4
PC 34:2
PC 35:0
PC 36:1
PC 37:1
PC 40:0
PC 40:4
PC 42:2
PC 42:5
PC 44:2
PC 44:4
PC O-39:0
PE 18:0_20:3
PE O-38:3
Plasmanyl-PC O-35:0
Plasmanyl-PC O-36:1
Plasmanyl-PC O-36:2
Plasmanyl-PC O-38:0
Plasmenyl-PC P-36:1
Plasmenyl-PE P-38:0
Plasmenyl-PE P-40:1
Plasmenyl-PE P-42:1
PS 38:1
SHexCer d18:1_22:0
SHexCer d18:1_24:0
SHexCer d36:2
SHexCer d44:2
SP d18:2
TG 18:1_18:1_24:0
-2 0 2 4
e)
SLC13A5 sTg brain
-log10(p-value)
Log2 (fold change from WT)
SLC25A1 sTg brain
-log10(p-value)
Log2 (fold change from WT)

Supplementary Figure 7. SLC13A5 sTg and SLC25A1 sTg mice display different lipid adaptation in the brain.

(a) Venn diagram showing overlap between SLC13A5 sTg (purple) and SLC25A1 sTg (orange) mice across statistically significant lipids (n=5 male mice per group).

(b) Heat-map showing the expression profile of dysregulated lipids (total of 4) found in SLC13A5 sTg and SLC25A1 sTg mice, as compared to WT littermates.

(c) Heat-map showing the expression profile of dysregulated lipids (total of 18) found in SLC13A5 sTg mice, as compared to WT littermates.

(d) Heat-map showing the expression profile of dysregulated lipids (total of 36) found in SLC25A1 sTg mice, as compared to WT littermates.

(e) Volcano plots displaying all quantified lipids in SLC13A5 sTg and SLC25A1 sTg brain, as compared to age-matched WT littermates. Statistically significant species are highlighted in purple (for SLC13A5 sTg) and orange (for SLC25A1 sTg). $P<0.05$ via Fisher's method with all other species in grey.

Mice were 2 month-old when analyzed.

a)

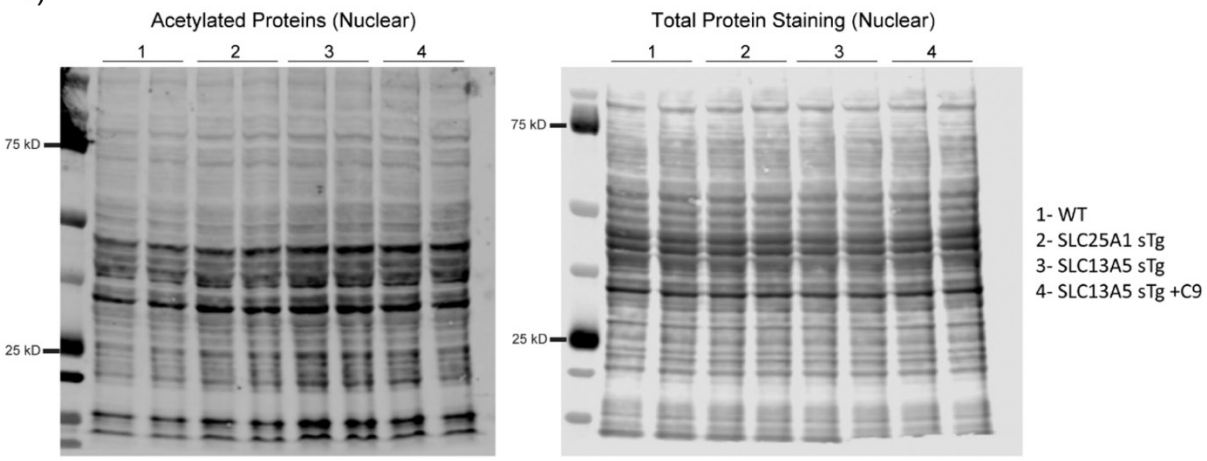
Acetylated Proteins (Nuclear)
1
2
3
4
75 kD
25 kD
Total Protein Staining (Nuclear)
1
2
3
4
75 kD
25 kD
1- WT
2- SLC25A1 sTg
3- SLC13A5 sTg
4- SLC13A5 sTg +C9

b)

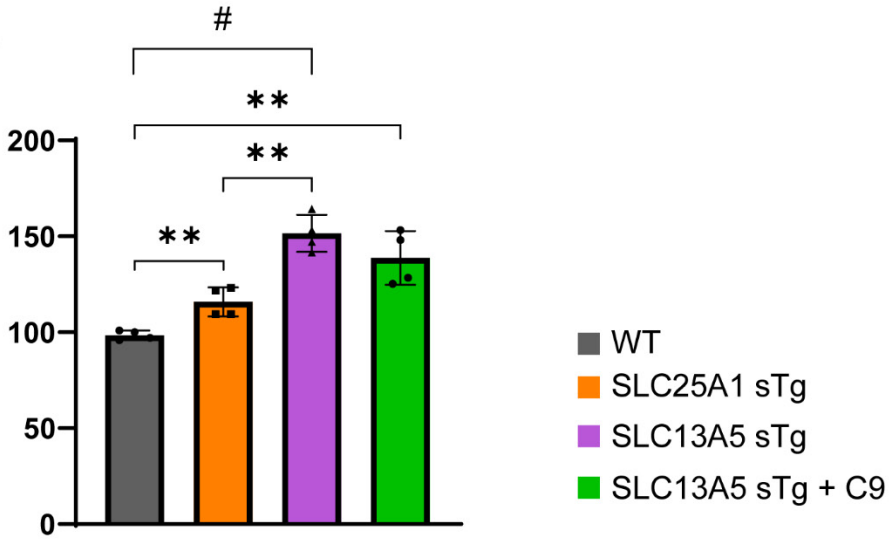
#
**
**
**
200
150
100
50
0
WT
SLC25A1 sTg
SLC13A5 sTg
SLC13A5 sTg + C9

c)

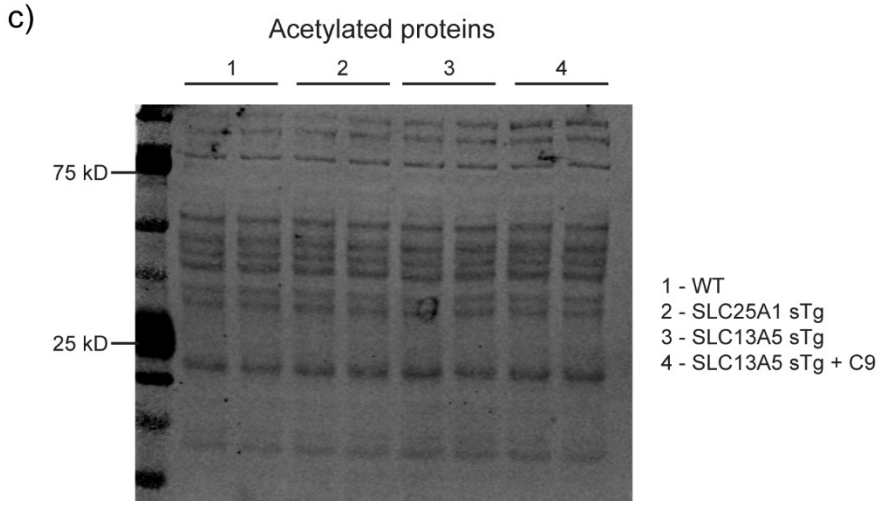
Acetylated proteins
1
2
3
4
75 kD
25 kD
1 - WT
2 - SLC25A1 sTg
3 - SLC13A5 sTg
4 - SLC13A5 sTg + C9

Supplementary Figure 8. The increased acetylation of the nucleus in SLC13A5 sTg mice is not rescued by C9.

(a-b) Western blot showing the profile of Nε-lysine acetylation in the nucleus isolated from the liver. Representative Western blot with total protein staining (a) and quantification (b) are shown. *C9*, Compound 9.

(c) Western blot showing the profile of Nε-lysine acetylation in the total liver lysate. *C9*, Compound 9.

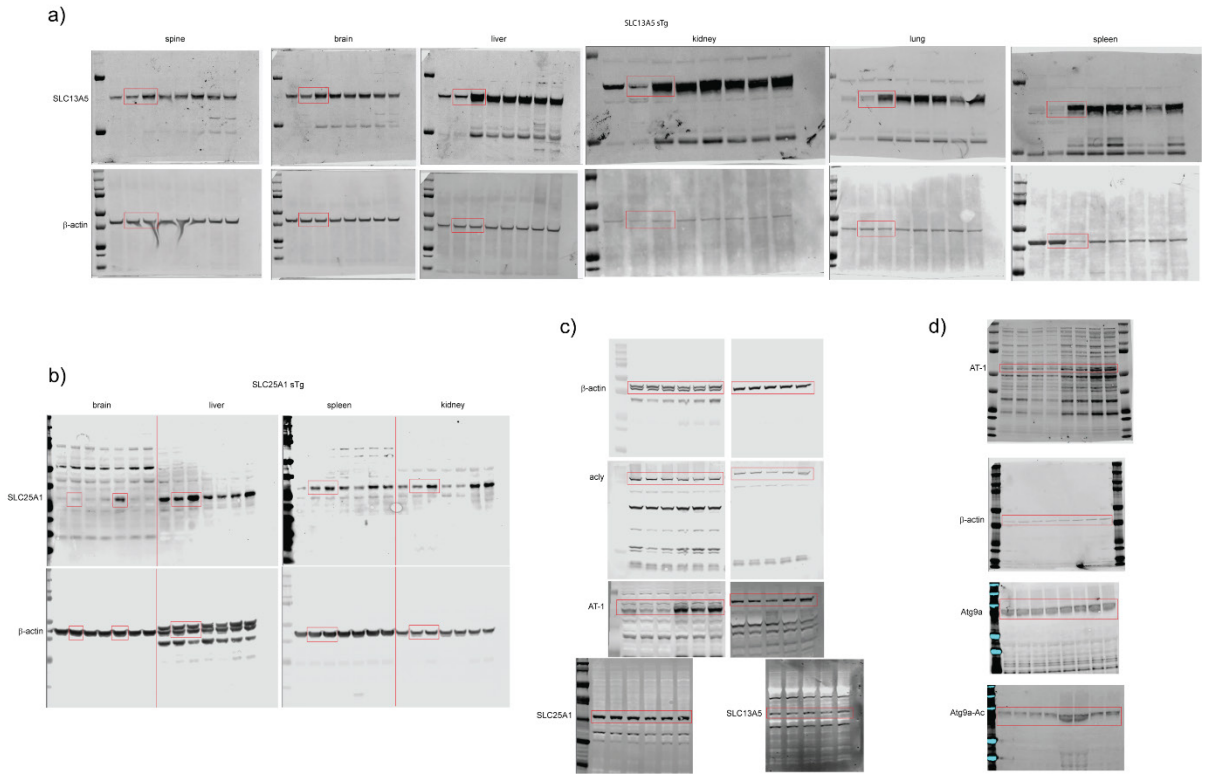

Supplementary Figure 9. Uncropped Western blots from Figure 1J (panel a and b), Figure 7b (panel c), Figure 7c and 7e (panel d).